

Spatial Log-Gaussian Cox process models and sampling paths: towards optimal design

Kenneth Flagg^{a,*}, John Borkowski^a, Andrew Hoegh^a

^a*Department of Mathematical Sciences, Montana State University, Bozeman, MT 59717*

Abstract

Goal of this paper (placeholder abstract—add some results when available). Evaluate a wide variety of path designs in terms design-based heuristics and model-based criteria for spatial prediction using Bayesian LGCP models. Identify promising path designs. Illuminate any relationships among design characteristics and predictive criteria that will be helpful for constrained optimization.

Keywords: log-Gaussian Cox process, optimal sampling, model-based design, spatial sampling design

1. Introduction

Spatial point process models have generally been infeasible because of their computational demands, but recent advances in Bayesian computing have made the Log-Gaussian Cox process (LGCP) an attainable model in practice (Rue et al., 2009; Lindgren et al., 2011; Illian et al., 2012; Simpson et al., 2016). These advances make it possible to fit LGCP models easily, without time-consuming Monte Carlo methods. In some applications, the entire point pattern is not fully observed due to variable sampling effort. This is referred to as a degraded point pattern (Chakraborty et al., 2011) and it is relatively simple to accommodate variable sampling effort in these models using modern Bayesian computing

*Corresponding author
Email address: kenneth.flagg@montana.edu (Kenneth Flagg)

tools (Yuan et al., 2017). However, the literature on optimal sampling for spatial point process models is in its infancy (Liu and Vanhatalo, 2020).

Point pattern data are routinely collected in species distribution studies and ordnance response projects. The data consist of the locations of events in some spatial region. These applications may use quadrat sampling or line-transect sampling, with transect sampling being more common. When the objective is to map where events occur in space, various spatial mapping procedures have been used. Traditionally these have involved aggregating the data to grid cell counts or computing moving averages. Aggregation has the downside of introducing arbitrary structure into the data by the choice of grid scheme or averaging window, and requires unnecessary computation effort (Simpson et al., 2016). Software is now available to fit spatial point process models to data acquired via distance sampling and simultaneously estimate the detection function (Johnson et al., 2014; R Core Team, 2019).

In ecological settings, sampling plans are often designed around the goal of estimating total abundance. Ordnance response surveys are typically designed to provide enough data to detect (but not necessarily map) intensity hotspots (USACE, 2015; Flagg et al., 2020). However, to our knowledge, there has been very little work done in deciding *where* to collect data when the goal is to map the intensity using a spatial point process model. While some ideas about the characteristics of a good point design apply to paths, creating an optimal path design is not as simple as connecting the points of a point design with line segments. There are many ways to connect points into a path, so optimal design criteria must apply to the whole path and not only to the waypoints. In this paper, we present a variety of sampling path designs and assess their optimality for mapping intensity using LGCP models.

1.1. Log-Gaussian Cox process

The log-Gaussian Cox process is an inhomogeneous Poisson process where the logarithm of the intensity function is a Gaussian process (Møller et al., 1998).

The LGCP provides a flexible model for mapping event intensity over space

using few parameters. Efficient Bayesian computation tools are available using INLA to approximate the posterior marginal distributions Rue et al. (2009), a finite element approach to represent the Gaussian process Lindgren et al. (2011), and pseudodata to approximate the point process likelihood Simpson et al. (2016).

1.2. Spatial design

Most classical sampling and design work has been done for points, or for small quadrats approximated as points, rather than for paths. In two-dimensional (geostatistical) model-based design, regularity is optimal for spatial prediction but randomness and a variety of interpoint distances are best for parameter estimation (Diggle and Lophaven, 2006). Inhibitory plus close pairs designs are a good compromise (Chipeta et al., 2017). Design-based approaches exist to spread points through high-dimensional design spaces (Borkowski and Piepel, 2009), and Latin hypercube sampling has space-filling characteristics (McKay et al., 1979; Hussian et al., 2011).

1.3. Space-filling curves

Another relevant area of research is in deterministic space-filling curves. These have been used in the design of dense or stretchable circuits (Ogorzalek, 2009; Ma and Zhang, 2016) and high-dimensional data visualization in bioinformatics (Anders, 2009). The Hilbert curve is simple to construct and the Peano curve is very flexible for filling irregular shapes (Fan et al., 2014). Space-filling curves are one-dimensional paths constructed iteratively; as the number of iterations goes to infinity, the limiting path has nonzero area and actually fills the space (Sagan, 1994). For applications we stop after a finite number of iterations.

1.4. Paths as sampling designs

The small body of literature on spatial sampling design for point pattern data has focused on line transects. Pollard et al. (2002) began with line transects and adaptively added zigzags in a species abundance survey.

The Visual Sample Plan software includes features to create systematic transects plans and augment plans with additional transects in regions lacking spatial coverage (Matzke et al., 2014). It helps the user choose the transect spacing to maximize the probability of detecting the presence of a hotspot of specified size and intensity. However, it does not employ criteria to optimize spatial prediction.

Liu and Vanhatalo (2020) provided one of the first explicit discussions of design in the context of spatial LGCP models. They used narrow quadrats (swaths along line-transects) as their sampling units. The transects were short relative to the size of the study region and not connected into a path.

2. Materials and methods

80 2.1. Evaluation Criteria

With an eye toward practical considerations of data collection, we present criteria to compare sampling strategies that impact LGCP posterior. We compare plans with (approximately) fixed path lengths, most of which avoid sharp turns. Data collection equipment (e.g. metal detectors) may have limited mobility, requiring minimizing the number or angle of turns.

One important characteristic in addition the total path length is the concept of spatial coverage, or how well the design represents the study site in the sense that all points in the region are close to observed locations. We measure this by the average distance between points in the site and points on the path. We define the distance between a point and the path as the distance between that point and the nearest point on the path, then take the average over all points in the study region. This can be roughly understood as the radius of a typical unsurveyed void.

The model-based criteria that we evaluate are the error in the posterior mean:

$$E[\mu|\mathbf{X}_S] - \int_{\mathcal{R}} \log[\lambda(u)]du/|\mathcal{R}|,$$

the mean squared prediction error (MSPE) of the log intensity surface:

$$E[(\mu + \mathbf{e}(u) - \log[\lambda(u)])^2 | \mathbf{X}_{\mathcal{S}}],$$

and the average prediction variance (APV) of the latent Gaussian process:

$$\text{Var}[\mathbf{e}(u) | \mathbf{X}_{\mathcal{S}}].$$

In the above notation, λ is the true realized intensity function, which is known
95 in the simulations.

The first criterion captures accuracy in the overall scale of the intensity surface. Large-magnitude errors in the mean imply that that model will predict overall too many or two few events. The other criteria reflect two important characteristics of a useful spatial prediction. First, deviation from the true
100 surface should be low, and is indicated by low MSPE. Second, the model's own assessment of prediction uncertainty will be used in practice to build trust in the inferences, so APV should be low.

2.2. Sampling design schemes

In this section, we present three variations of parallel line transect designs
105 and three schemes that produce more complex designs. To clarify terminology, a *path* or *design* is a realized set of one or more connected components that has length but not area. The paths considered in this work are constructed as sequences of line segments. A *design scheme*, or simply *scheme*, is procedure for generating designs with some shared characteristics. Figure 1 illustrates a
110 selection of designs from these schemes.

2.2.1. Parallel line transects

Parallel straight-line transects are common in ordnance response studies and in ecological studies using distance sampling. Systematic designs are common because they provide good spatial coverage in the sense that any point in the
115 study region has an a priori known maximum distance from the path. For point designs, systematic designs are optimal for prediction, simple random samples

are optimal for estimation, and inhibitory with close pairs designs are becoming a popular compromise. We adapt all of these to the parallel line transect setting. We use line transects running north-south, with three methods of choosing the horizontal coordinate: simple random sample (SRS), systematic with a random starting point and even spacing, and inhibitory plus close pairs. Figure 1 (left column) shows an example of each scheme with 25 transects.

2.2.2. Parallel serpentine transects

One simple way to observe a greater variety of locations and different directions is to add lateral “zigzags” to transects. We include alternate right and left turns at right angles to create serpentine transects. This could decrease prediction variance because more of the path will be close to each point in the study area than would be under a line transect design with similar total distance. They will also improve estimation of the covariance function in the presence of anisotropy. Figure 1, top right, shows two examples.

2.2.3. Latin hypercube sampling

Random Latin hypercube sampling (LHS) produces a design that spreads discrete points through a (potentially high-dimensional) design space, ensuring that the full range of each dimension is included while remaining balanced and keeping the number of points small (McKay et al., 1979). This is done by partitioning each dimension into a specified number k of intervals (thus stratifying a d -dimensional design space into k^d cells), selecting a Latin hypercube design to determine which k cells will contain a design point, and then drawing each design point from a uniform distribution over its cell. In two dimensions, this scheme produces point designs with good spatial coverage properties. We use the LHS design as waypoints for a path. Because longer distance typically brings increased costs, we treat this as a traveling salesperson problem (TSP) and use the shortest path through the waypoints as our design. This LHS-TSP scheme produces paths that have many sharp corners but leaves few large voids (example in Figure 1, bottom left). A downside of this design scheme is that

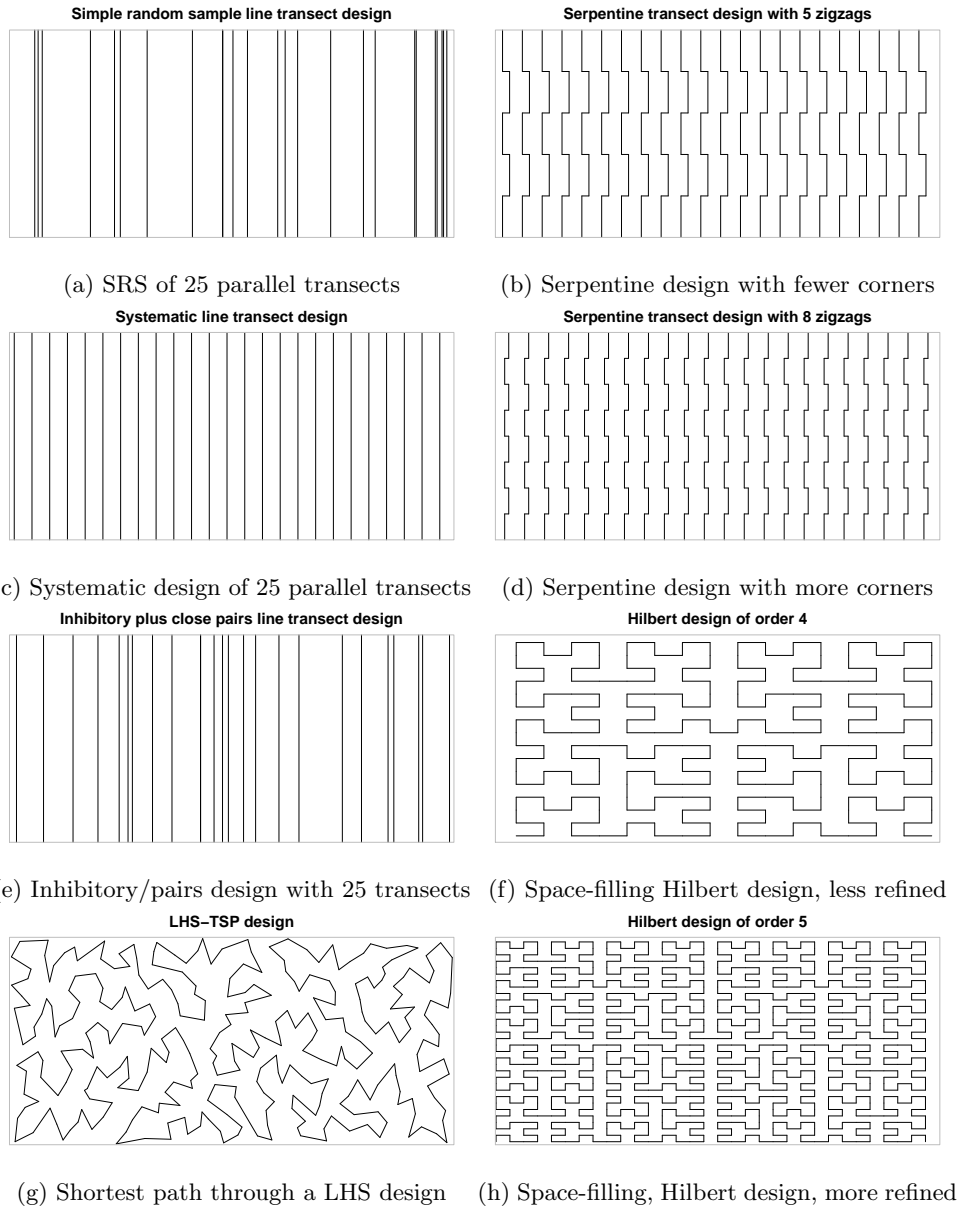


Figure 1: Examples of plans from six design schemes. Except for the Hilbert curve of order 5, all of these plans have approximately the same total length.

the length cannot be specified directly, and only certain distances are possible depending on the number of bins used.

Waypoints are generated by the `lhs` R package Carnell (2020) and connected into a the shortest path by the `TSP` package (Hahsler and Hornik, 2020).

150 *2.2.4. Space-filling curves*

As a representative of space-filling curves, we use the Hilbert curve scaled to fit the study site. These designs have many short segments meeting at right angles. The only parameter of this design scheme is the order, or number of iterations used in refining the curve. Each iteration increases the length and complexity of the design. This produces a deterministic design, so a random offset is added to vary which points are observed. The Hilbert curve is generated by `HilbertVis` R package (Anders, 2009).

2.3. *Model fitting*

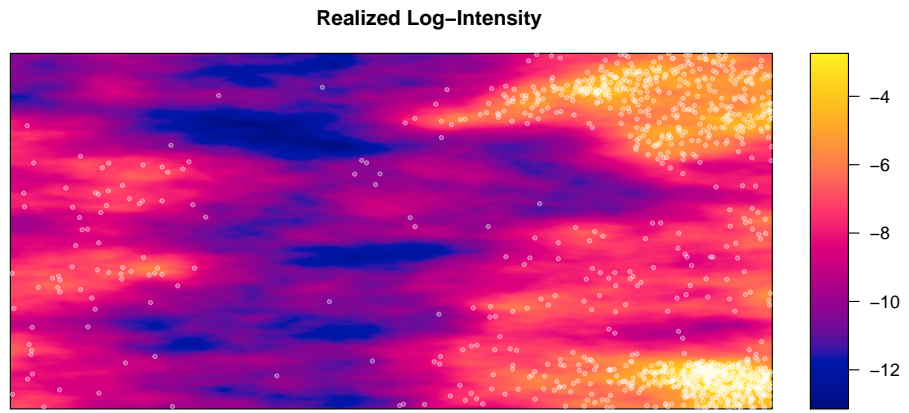
We fit the spatial LGCP model using nested integrated Laplace approximations and the R-INLA package (Rue et al., 2009; Blangiardo and Cameletti, 2015). The Gaussian process is approximated using a finite element approach (Lindgren et al., 2011). The point pattern is modeled by pseudodata placed at the events and the finite element nodes (Simpson et al., 2016). This procedure allows fast and accurate approximation of the posterior distribution.

165 **3. Simulation Study**

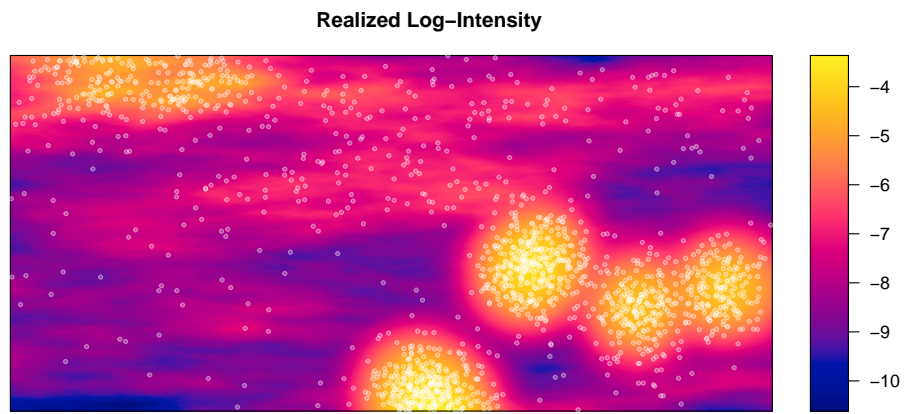
We simulate 100 designs from each of six schemes. All events within a 2 unit radius of the path are observed. The whole experiment is repeated for 5 realizations from each of two data generating models.

3.1. *Study site*

170 We consider a fictitious site \mathcal{R} with the simple shape of a 1500 unit by 700 unit rectangle. In this site, we simulate two data generating models that produce random intensity functions with hotspots. First, a LGCP with latent GP mean



(a) Realized LGCP log-intensity



(b) Realized LGCP with Clusters log-intensity

Figure 2: The realized intensity function (natural log scale) and complete point pattern from a LGCP, and from a LGCP superposed with a cluster process.

$\mu = \log(250/|\mathcal{R}|) = -8.34$ and Matérn covariance function with $\nu = 1$, $\sigma = 2$, and range = 200. This model produces relatively unstructured hotspots due to
175 large variability in the GP. Figure 2a shows an example realization from this process.

Second, a two-stage cluster process and a LGCP are superposed. The cluster process (a Neyman-Scott or, more specifically, a Thomas process) is constructed as follows. The number of clusters is Poisson-distributed with mean 3. The
180 number of events per cluster is Poisson-distributed with mean 200. The cluster centers are distributed uniformly over \mathcal{R} . Events come from a bivariate normal distribution with mean equal to the cluster center and variance $\Sigma = \tau^2 \mathbf{I}$, $\tau = 50$. The LGCP component has $\mu = \log(250/|\mathcal{R}|) = -8.34$ and Matérn covariance with $\nu = 1$, $\sigma = 1$, and range = 200. This model is based upon the typical conceptual model of a firing range, with a background process (represented by the
185 LGCP) and a small number of higher-intensity foreground clusters containing the events of interest (example in Figure 2b). As a shorthand, we refer to this generative process as LGCP with Clusters.

The LGCP generating process matches the model we fit to the realized
190 data. The model should both produce accurate predictions and have low bias in the posterior means of the parameters. On the other hand, the parameters of the LGCP with Clusters process will not correspond to the LGCP model parameters, but we anticipate that in general the latent GP in the LGCP model will still accurately predict the log-intensity function.

195 *3.2. Path design schemes*

The simulation uses each of the design schemes discussed in Section 2.2. The design parameters for each scheme are varied to create four different levels of survey effort: low, medium, high, and very high. Within each effort level, the total length or distance traveled is comparable across all schemes. The inhibitory
200 plus close pairs scheme and the serpentine scheme are further varied to employ different numbers of pairs and different numbers of zigzags, respectively. Table 1 provides an overview of the different settings.

Table 1: Design schemes used in the simulation study. The table presents the design parameters, distance travelled along the path, percent of the study area surveyed, and average distance to the path under each of four survey effort levels. The average distance to the path varies due from design to design, and is presented as average (SD).

* Variable area due to overlapping segments, reported as average (SD).

** Variable distance surveyed, reported as average (SD).

Scheme	Low Effort	Medium Effort	High Effort	Very High Effort
SRS	10 transects Length: % Surveyed: Avg. Dist. to Path:	25 transects 7000 units 6.46% (0.202%)* 29.7 (6.01)	50 transects 35000 units 12.5% (0.331%)* 15.0 (1.99)	70 transects 49000 units 17.2% (0.459%)* 10.8 (1.44)
Systematic	10 transects Length: % Surveyed: Avg. Dist. to Path:	25 transects 7000 units 2.68% 6.70% 38.4 (0.866)	50 transects 35000 units 13.4% 7.56 (0.0307)	70 transects 49000 units 18.7% 5.40 (0.0164)
Inhibitory, 10% Close Pairs	9 transects 1 paired Length: % Surveyed: Avg. Dist. to Path:	23 transects 2 paired 7000 units 6.53% (0.172%)* 20.8 (1.82)	45 transects 5 paired 35000 units 12.8% (0.314%)* 10.6 (1.24)	63 transects 7 paired 49000 units 17.5% (0.427%)* 7.64 (0.576)
Inhibitory, 20% Close Pairs	8 transects 2 paired Length: % Surveyed: Avg. Dist. to Path:	20 transects 5 paired 7000 units 6.56% (0.157%)* 22.0 (2.97)	40 transects 10 paired 35000 units 12.8% (0.303%)* 11.4 (1.70)	56 transects 14 paired 49000 units 17.6% (0.368%)* 8.26 (0.826)
Serpentine, 5 Zigzags	7 transects 75 unit offset Length: % Surveyed: Avg. Dist. to Path:	22 transects 23.9 unit offset 7000 units 6.68% 43.2 (1.83)	47 transects 11.2 unit offset 35000 units 13.4% 7.79 (0.0508)	67 transects 7.84 unit offset 49000 units 18.7% 5.51 (0.0309)
Serpentine, 8 Zigzags	7 transects 42.9 unit offset Length: % Surveyed: Avg. Dist. to Path:	22 transects 13.6 unit offset 7000 units 6.67% 44.5 (2.03)	47 transects 6.38 unit offset 35000 units 13.3% 7.76 (0.0328)	67 transects 4.48 unit offset 49000 units 18.7% 5.50 (0.0271)
LHS-TSP	50 bins Length: % Surveyed: Avg. Dist. to Path:	300 bins 7177 (189) units** 2.73% (0.0722%)** 43.5 (1.44)	1200 bins 17191 (168) units** 6.51% (0.0632%)** 17.4 (0.186)	2400 bins 34196 (225) units** 12.9% (0.0835%)** 8.63 (0.0683) 48433 (342) units** 18.2% (0.127%)** 6.08 (0.0562)
Hilbert Curve	3rd Order Length: % Surveyed: Avg. Dist. to Path:	4th Order 8581 units 3.27% 37.3 (1.95)	5th Order 35025 units 6.634% 17.9 (0.480)	6th Order 70121 units 26.47% 8.77 (0.113) 4.37 (0.0382)

The parallel transect schemes have 10, 25, 50, or 70 line transects running north-south. We expect the simple random sample scheme to produce high prediction variance and large prediction error in big gaps between transects.
205 The systematic sample scheme uses a uniformly-distributed starting point and constant spacing between adjacent transects. We expect systematic transects to provide low bias and moderate prediction variance. However, this scheme can miss structures at certain sizes because no transects are close to each other in the east-west direction.
210

For the inhibitory plus close pairs line transect scheme, we vary the numbers of paired and unpaired transects. The total number of transects is 10, 25, 50, or 70, with 10% and 20% of the transects (rounded to the nearest integer) as redundant members of a pair. The remaining primary transects are placed according to a one-dimensional Strauss process (Strauss, 1975; Kelly and Ripley, 1976). The Strauss attraction parameter is set at $\gamma = 0.05$ and the radius for counting pairs is 1500 units divided by the total number of transects. Then each redundant transect is randomly paired to a primary transect, and placed within the pair radius of the primary transect according to a uniform distribution.
215
220 We expect this scheme to have intermediate performance between the simple random sample and the systematic line transect schemes.

The serpentine transect scheme has 7, 22, 47, or 67 transects running north-south with constant east-west spacing and a random starting point for the first transect. The number of zigzags (north-south segments) is 5 or 8 per transect, and the pedicular offset is set so the the total east-west distance equals the length of three north-south line transects. Thus, the serpentine designs traverse the same length as the line transect designs. These designs should result in smaller prediction errors and lower variance farther from the path, compared to line-transect designs.
225

230 Our Latin hypercube sampling/traveling salesperson (LHS-TSP) scheme uses 50, 300, 1200, or 2400 bins to generate the waypoints. Preliminary experimentation found that these bin numbers produced total lengths similar to the line-transect schemes. The LHS-TSP scheme is expected to result in small

prediction errors and low prediction variance per unit distance traveled. How-
235 ever, the designs will have many sharp corners and may leave some large voids.

The Hilbert curve scheme uses a random starting point and a Hilbert curve
of order 3, 4, 5, or 6. The path length is a deterministic function of the order
and differs greatly among curves of different orders. These orders yield lengths
similar to the lengths of the transect designs. Hilbert designs should provide low
240 prediction variance, but have lots of short segments.

3.3. Model specification

The same Bayesian LGCP model is fit to each observed dataset. The ob-
served point pattern \mathbf{x} is a realization of \mathbf{X} , a Poisson process on \mathcal{R} with intensity
 $\lambda(u)$. The intensity is modeled as $\log[\lambda(u)] = \mu + \mathbf{e}(u)$. The spatial error term \mathbf{e}
245 is a Gaussian process with mean $\mathbf{0}$ and a Matérn covariance function with fixed
 $\nu = 1$.

The intercept μ has a $\text{Unif}(-\infty, \infty)$ prior. The covariance parameters σ and
 ρ have a PC prior with $\Pr(\sigma > 3) = 0.1$ and $\Pr(\rho < 100) = 0.1$ (Fuglstad et al.,
2019; Simpson et al., 2017).

250 The Gaussian process prediction surface is approximated on the finite el-
ement mesh shown in Figure 3. The GP is predicted at the nodes (points)
and is linearly interpolated elsewhere. The nodes are weighted according to the
area of their dual cells (grey outlines) and used for numerical integration of the
likelihood (Lindgren et al., 2011). This mesh is adequately fine to model the
255 large-scale trends in the surface while keeping the computing time well under a
minute for each model fit.

4. Results

4.1. Initial Observations

In describing the results, we focus on one LGCP dataset and one LGCP
260 with Clusters dataset (Figure 2). The results are similar for all datasets (see
the online supplement.)

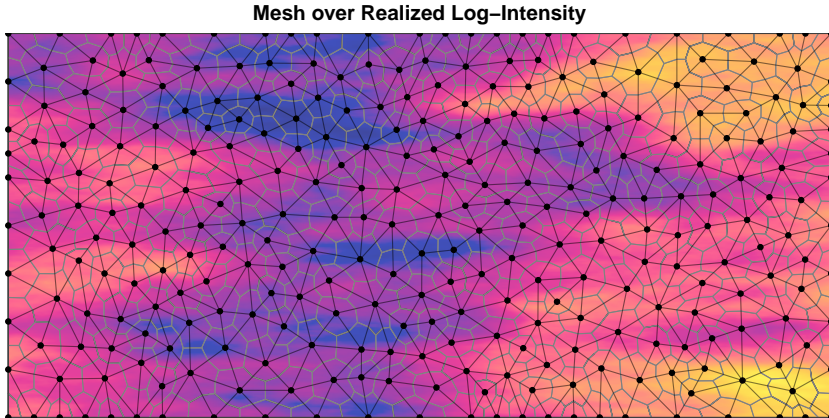
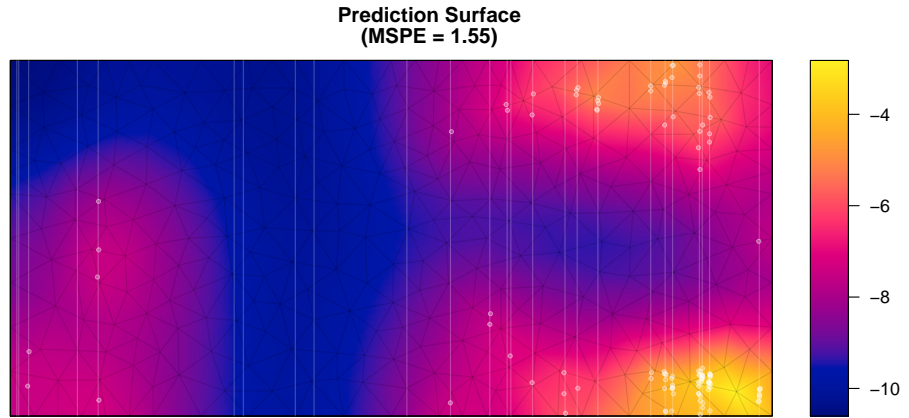


Figure 3: Illustration of the mesh used to approximate the latent GP. The mesh nodes are used in a numerical integration scheme where they are weighted by the area of their dual cells (outlined in grey).

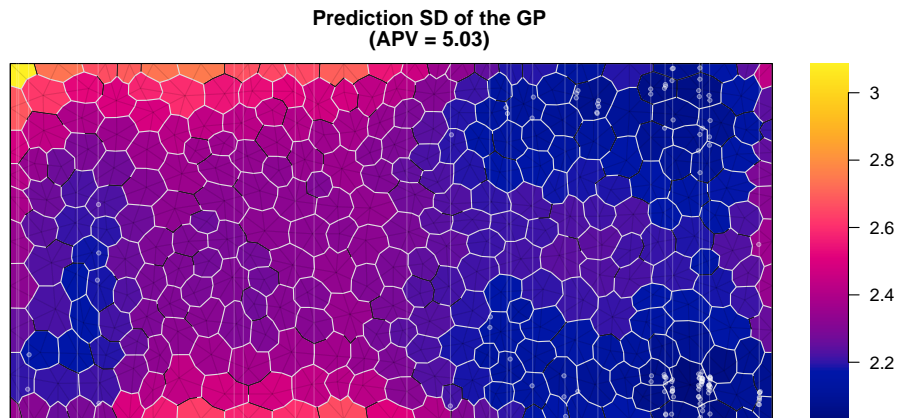
Figure 4 shows an example where the model does well at predicting the intensity of the realized LGCP from data observed along one of the SRS paths. In the figure, the path appears in white and the observed events are shown as white dots. The posterior predicted mean of the log-intensity (top panel) accurately captures the large-scale features, but smooths out much of the small-scale variation. The bottom panel shows the prediction standard deviation for each mesh node. The SD ranges from 2.0 to 3.1, and is lowest near observed events. SD increases farther from observed events, including in places where the surveyed area was observed to contain no events.

This same survey plan also did well for the LGCP with Clusters dataset, with the model accurately capturing the large-scale details of the intensitiy function, including two of the circular hotspots corresponding to clusters (Figure 5a). However, it also smoothed the surface quite a bit, notably merging the two overlapping clusters into a single oblong hotspot.

Most plans yielded similar prediction surfaces, capturing the large-scale trends, and having the least uncertainty near observed events. Results varied in accuracy at the most extreme peaks and valleys of the itensity function and in overall SD across the study region.

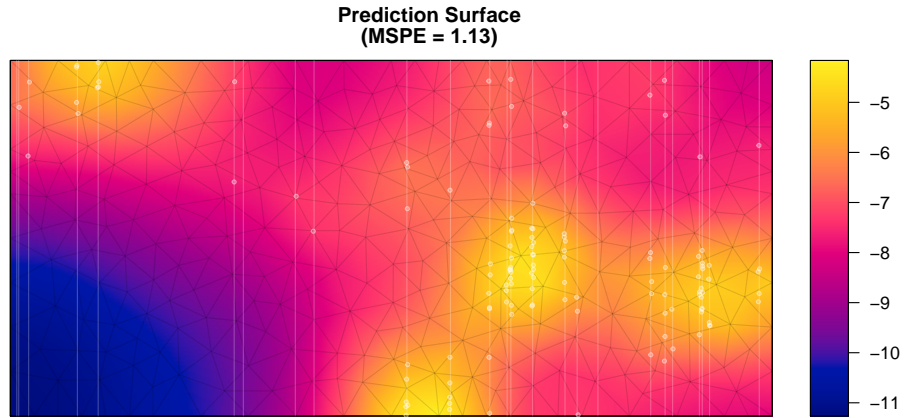


(a) Predicted log-intensity

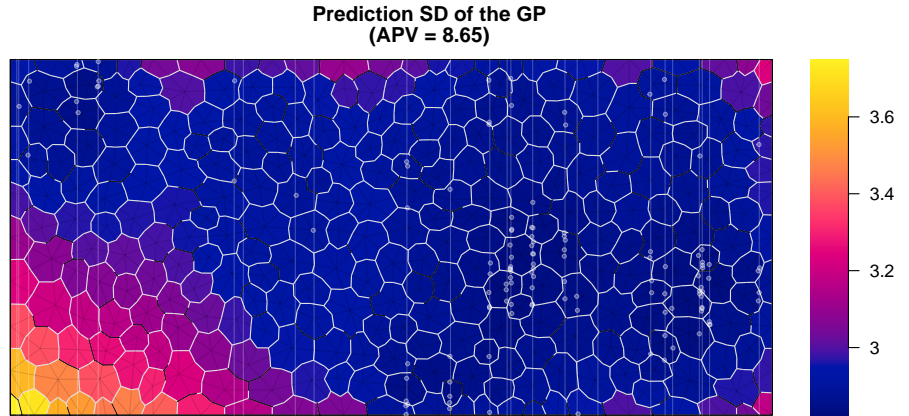


(b) Prediction SD

Figure 4: Predicted log-intensity function and prediction standard deviation using data observed via a SRS of line transects. The SD is shown for each finite element node. This example is a medium-effort plan applied to a LGCP dataset.



(a) Predicted log-intensity



(b) Prediction SD

Figure 5: Predicted log-intensity function and prediction standard deviation using data observed via a SRS of line transects. The SD is shown for each finite element node. This example is a medium-effort plan applied to a LGCP with Clusters dataset.

280 However, a small number of model fits suffered from apparent edge effects.
For example, Figure 6 shows the prediction surface resulting from a serpentine
transect plan. The predicted log-intensity has a hotspot of extremely large
values in the southeast corner (notice the color scale). The hotspot is driven
by two nodes on the boundary with very large prediction values. Another, less
285 extreme, edge effect is present in the northeast corner.

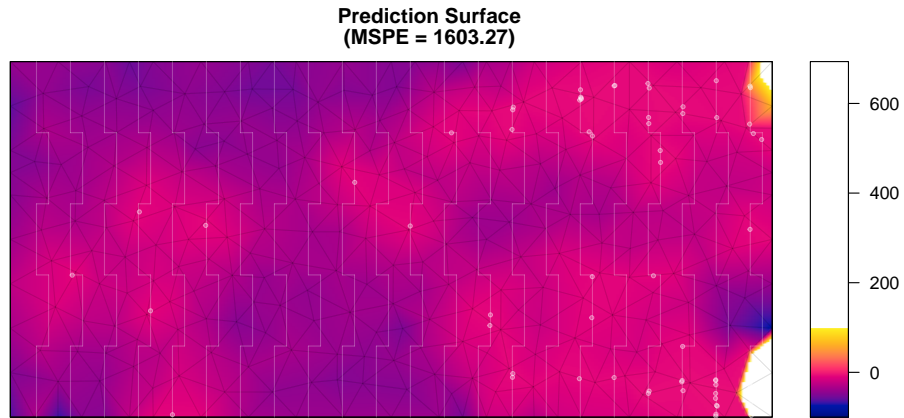
The next sections compare the schemes in terms of model-based criteria
applied to one realized LGCP dataset and one realized LGCP with Clusters
dataset.

4.2. LGCP simulation results

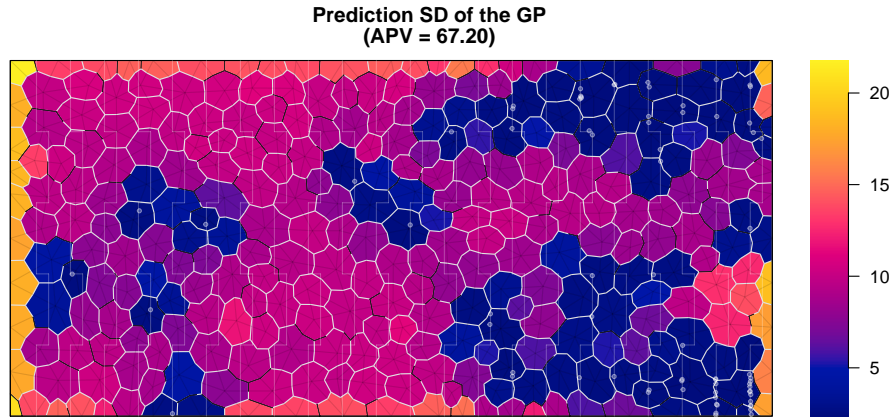
290 Considered across all survey plans applied to one LGCP dataset, both MSPE
and APV had right-skewed distributions. Thus we use logarithmic scales for
plots and summarize them using the median and interquartile range (IQR).
Median MSPE decreases with increasing path distance, leveling off around be-
tween the medium and high effort levels (Figure 8a). Variability (IQR) of MSPE
295 also decreases as effort increases. Prediction surfaces with edge effects form a
cluster of large, outlying MSPE values. At all levels of effort, systematic designs
had the least variability in MSPE. The lowest-MSPE prediction surfaces result
from the longest Hilbert designs, but the distributions of MSPE are similar for
all schemes at the high and very effort levels. Overall, the differences among
300 the different schemes with respect to median MSPE are much less than the
variability in MSPE within each effort level. The results are largely the same
for APV (Figure 8b).

4.3. LGCP with Clusters simulation results

For the LGCP with Clusters dataset, MSPE and APV again had right-
305 skewed distributions. Median MSPE decreases as effort increases (Figure 9a).
Variability in MSPE is roughly constant across effort levels. The systematic
scheme had the lowest median MSPE for low and medium effort and low IQR
for all effort levels, while the serpentine and Hilbert schemes have the lowest



(a) Predicted log-intensity. The color scale is truncated at 100, but reaches a maximum of 692.



(b) Prediction SD

Figure 6: Predicted GP surface and prediction SD using data observed via a serpentine transect plan. The prediction has an apparent edge effect in the southeastern corner. The SD is high across much of the site. This example is a medium-effort plan applied to a LGCP dataset.

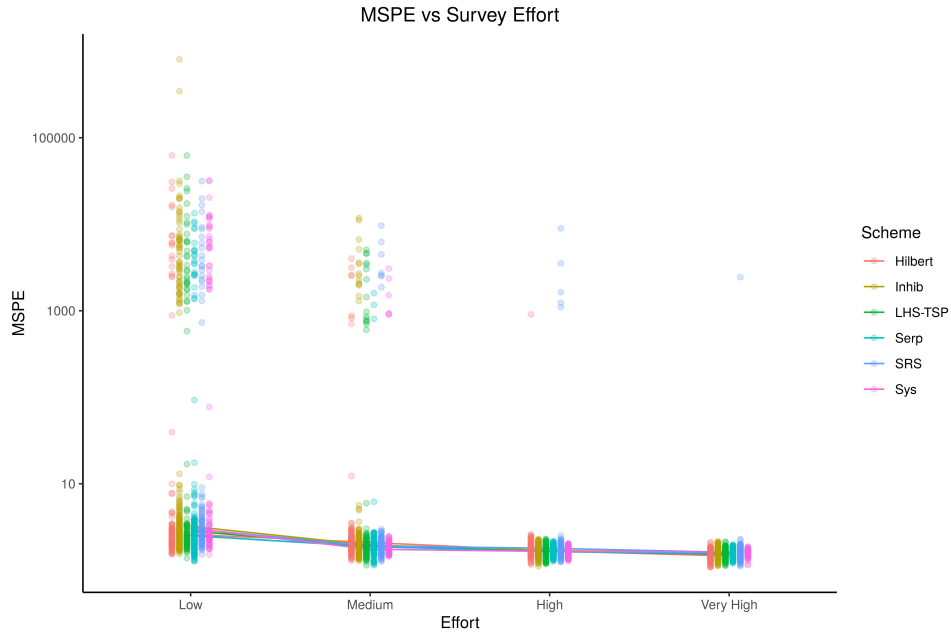


(a) MSPE distribution for one LGCP dataset

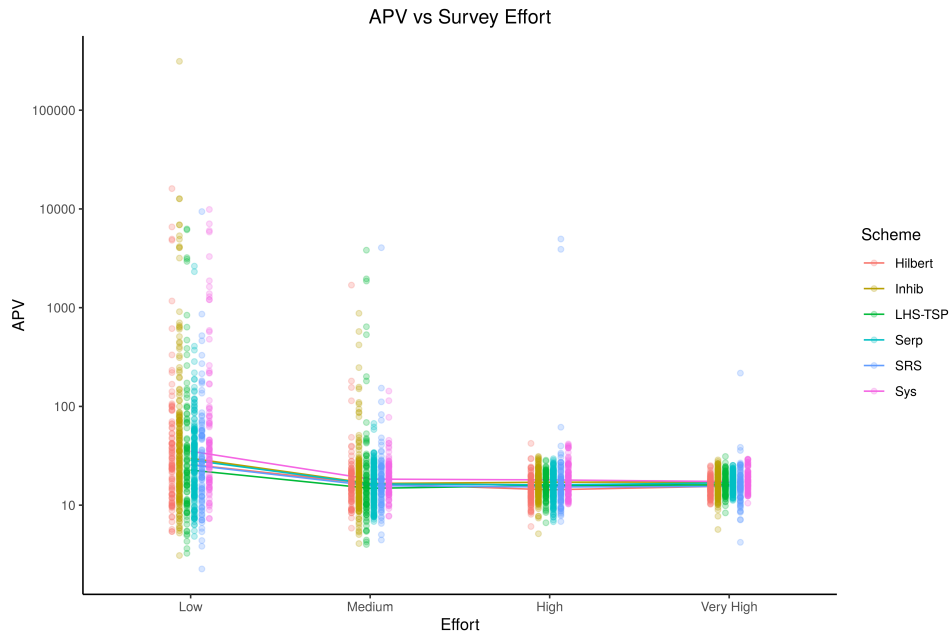


(b) MSPE distribution for one LGCP with Clusters dataset

Figure 7: Plots of the distribution of high and low mean squared prediction error (MSPE) vs survey effort for each plan applied to one realization of a LGCP and one realization of a LGCP with Clusters.



(a) MSPE vs survey effort for one LGCP dataset



(b) APV vs survey effort for one LGCP dataset

Figure 8: Plots of mean squared prediction error (MSPE) and average prediction variance (APV) vs survey effort for each plan applied to one realization of a LGCP. Line segments connect the median at each effort level. The plots are paneled by design scheme.

median at high and very high effort. However, difference between schemes are
310 much less than differences across survey effort. At low effort, the distribution
of APV has a long tail. Otherwise there are little difference in distribution of
APV across schemes or effort (Figure 9b).

4.4. Spatial coverage

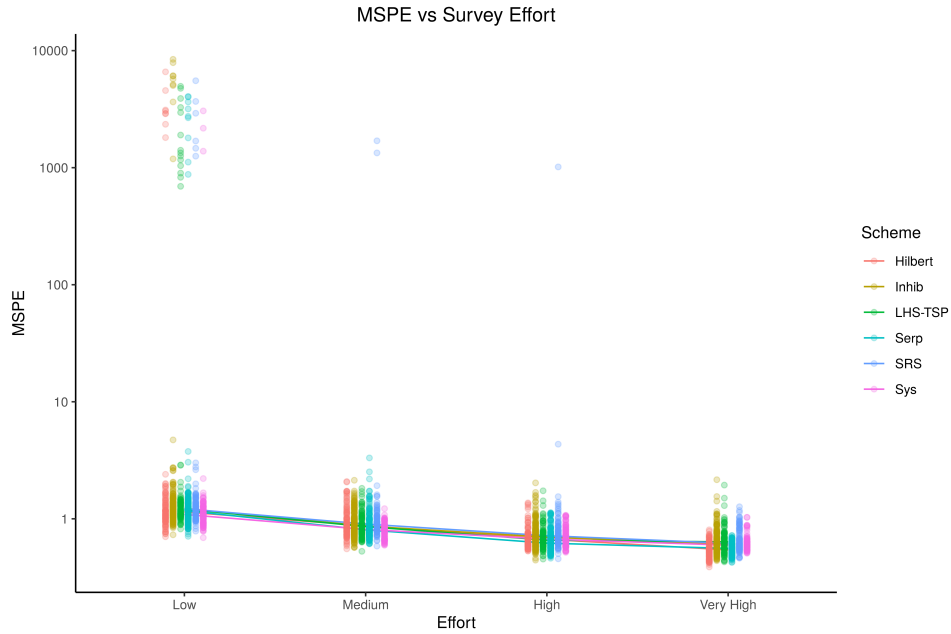
While the above results suggest the choice of design is relatively unimportant
315 and the distance traveled is the main driver of the quality of the spatial
predictions, it is important to consider that all of the design schemes ensure
the path is distributed across the entire study region. Designs that leave large
unexplored voids will not perform as well.

As an example, Figure 10 shows the results of using a systematic sample of
320 50 parallel transects in the western 20% of the study site. This design traverses
a distance of 35000 units but leaves most of the site far from the observed path.
As a result, the predicted log-intensity is flat near the GP posterior mean of
−8.71 over most of the site, rendering the prediction mostly useless.

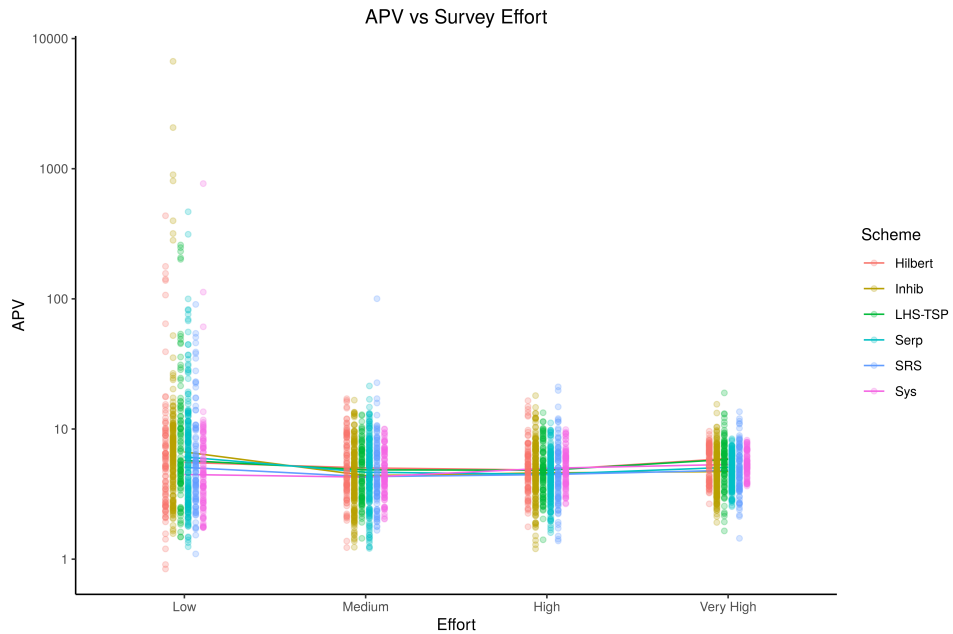
The problem with this example is easily explained in terms of the average
325 distance between the path and arbitrary points in the study site. This example
design has an average distance from the path of 486 units; the designs used in
the simulation study all had average distances to the path under 130 (with most
under 50).

4.5. Augmenting a poor-performing design

Even a poor-performing design could be used as a starting point for sequential
330 design. As a simple illustration, we augment the design from Figure 6 with
some additional sampling effort in the eastern part of the site, where the edge
effects were seen in the prediction surface. The total distance surveyed increases
from 17500 to 20180 units, while the predicted log-intensity surface is much more
335 accurate (Figure 12). MSPE decreases from 1600.57 to 2.48 and APV improves
from 67.20 to 11.02. Across the site, the prediction standard deviation is lower
than before, and is now highest around the edge of the western half. If we were

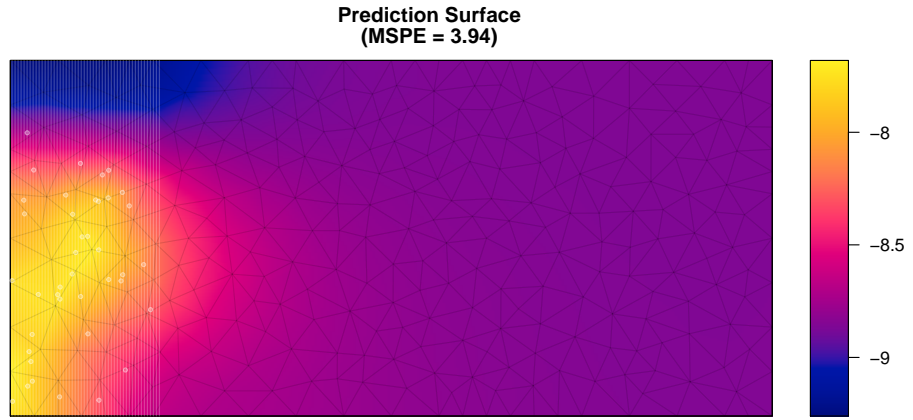


(a) MSPE vs survey effort for one LGCP with Clusters dataset

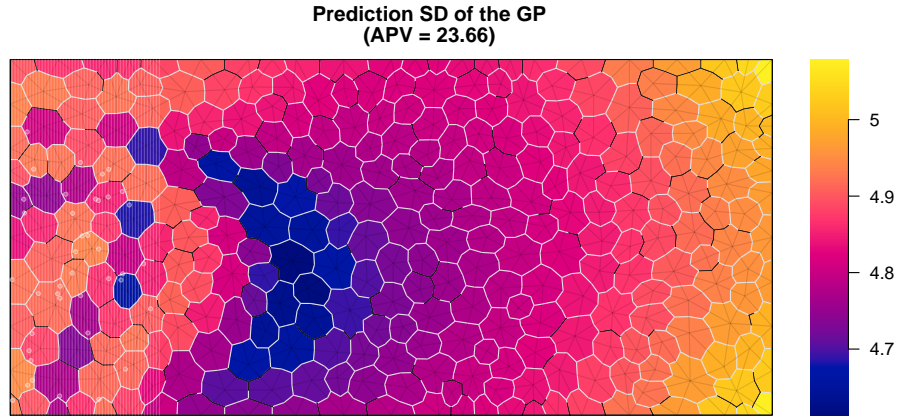


(b) APV vs survey effort for one LGCP with Clusters dataset

Figure 9: Plots of mean squared prediction error (MSPE) and average prediction variance (APV) vs survey effort for each plan applied to one LGCP with Clusters dataset. Line segments connect the median at each effort level. The plots are paneled by design scheme.

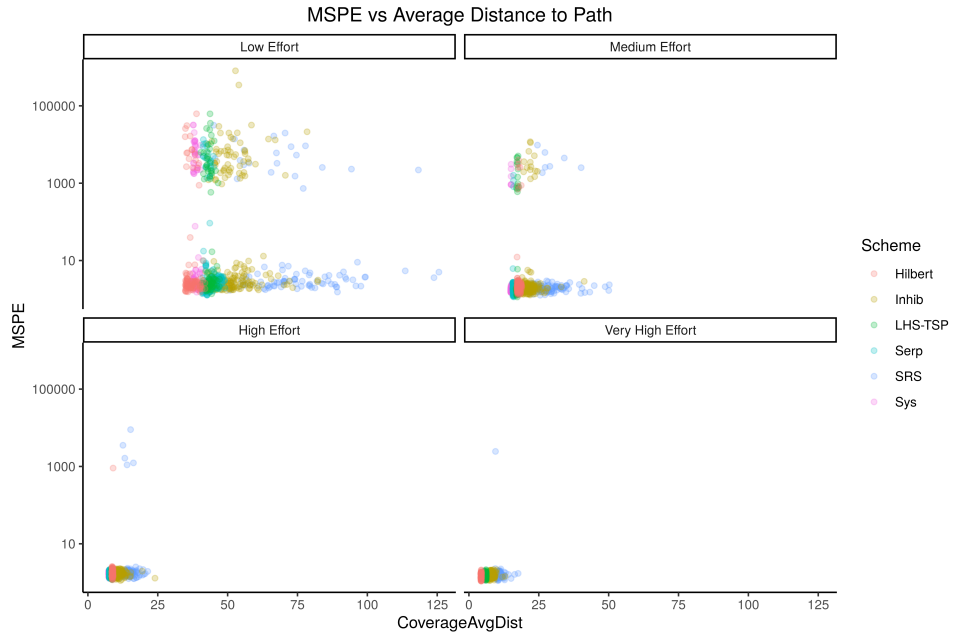


(a) Predicted log-intensity

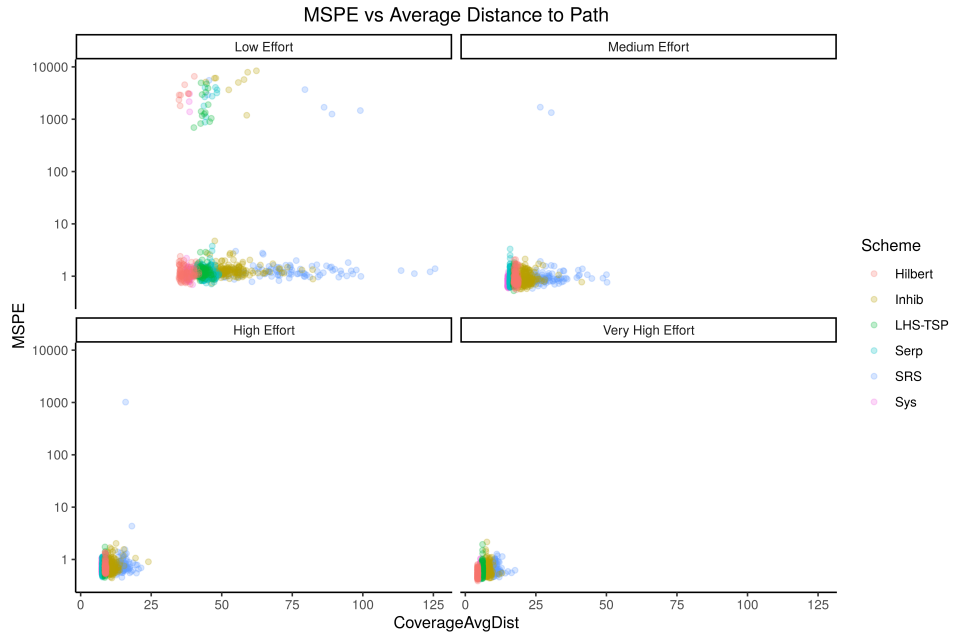


(b) Prediction SD

Figure 10: Predicted log-intensity function and prediction standard deviation using data observed via a systematic sample of a small section of the site. The SD is shown for each finite element node.



(a) MSPE vs coverage for one LGCP dataset



(b) MSPE vs coverage for one LGCP with Clusters dataset

Figure 11: MSPE plotted against the maximum distance from any point in the site to its the nearest point on the path. As survey effort increases, the cloud of points drifts down (lower MSPE) and to the left (lower average distance to the path).

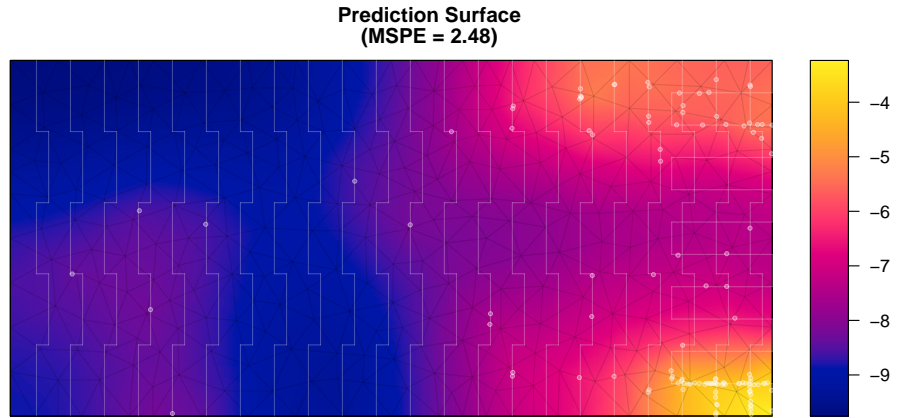
to continue adding segments to the path, giving some attention to the western portion of the site could further improve the prediction.

³⁴⁰ **5. Discussion**

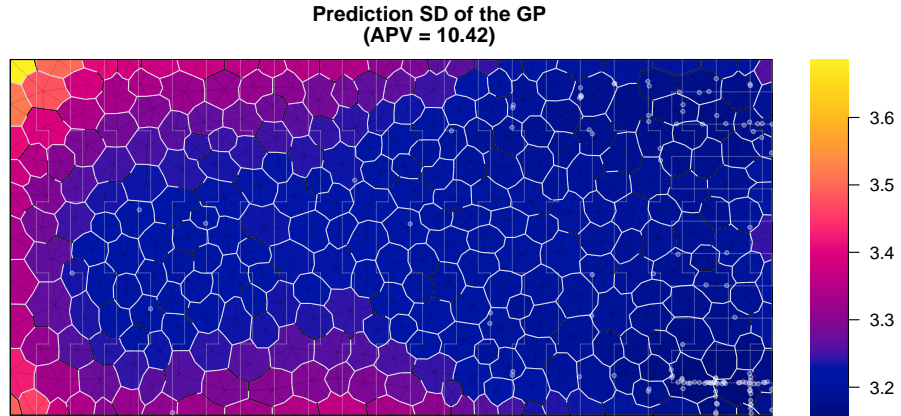
- increasing uncertainty along path — reasonable, path is narrow, could be events just out of detection range
 - convergence problems/large variance solution is more data collection?
 - discuss starting points for optimization and sequential design
- ³⁴⁵ ● practical issue: path will be smoothed, no instantaneous direction changes at corners, equipment may have limitations which is why we looked at number and distribution or turn angles
- could incorporate turns into loss function or use multi-objective optimization (Lark, 2016)

³⁵⁰ **6. Conclusions**

- for accuracy, choice of scheme does not matter much as long as it provides spatial coverage
 - of the schemes considered here, only transect schemes have flexibility in distance and/or a priori known distance
- ³⁵⁵ ● corners and regularity important for short paths to avoid model fitting problems (Hilbert or serpentine)
- systematic line-transects provide best spatial coverage but require many transects for good model performance
 - tradeoff useable posterior and simple designs



(a) Predicted log-intensity



(b) Prediction SD

Figure 12: Predicted log-intensity function and prediction standard deviation using data observed via a serpentine transect design augmented post-hoc. The SD is shown for each finite element node.

³⁶⁰ **References**

- Anders, S., 2009. Visualisation of genomic data with the Hilbert curve. *Bioinformatics* doi:10.1093/bioinformatics/btp152.
- Blangiardo, M., Cameletti, M., 2015. Spatial and Spatio-temporal Bayesian Models with R-INLA. Wiley.
- ³⁶⁵ Borkowski, J.J., Piepel, G.F., 2009. Uniform designs for highly constrained mixture experiments. *Journal of Quality Technology* 41, 35–47.
- Carnell, R., 2020. lhs: Latin Hypercube Samples. URL: <https://CRAN.R-project.org/package=lhs>. R package version 1.0.2.
- Chakraborty, A., Gelfand, A.E., Wilson, A.M., Latimer, A.M., Silander, J.A.,
³⁷⁰ 2011. Point pattern modelling for degraded presence-only data over large regions. *Journal of the Royal Statistical Society: Series C (Applied Statistics)* 60, 757–776.
- Chipeta, M., Terlouw, D., Phiri, K., Diggle, P., 2017. Inhibitory geostatistical designs for spatial prediction taking account of uncertain covariance structure.
³⁷⁵ *Environmetrics* 28.
- Diggle, P., Lophaven, S., 2006. Bayesian geostatistical design. *Scandinavian Journal of Statistics* 33, 53–64.
- Fan, J.A., Yeo, W.H., Su, Y., Hattori, Y., Lee, W., Jung, S.Y., Zhang, Y., Liu, Z., Cheng, H., Falgout, L., Bajema, M., Coleman, T., Gregoire, D., Larsen,
³⁸⁰ R.J., Huang, Y., Rogers, J.A., 2014. Fractal design concepts for stretchable electronics. *Nature communications* 5, 3266.
- Flagg, K.A., Hoegh, A., Borkowski, J.J., 2020. Modeling partially surveyed point process data: Inferring spatial point intensity of geomagnetic anomalies. *Journal of Agricultural, Biological and Environmental Statistics* 25, 186–205.

- 385 Fuglstad, G.A., Simpson, D., Lindgren, F., Rue, H., 2019. Constructing priors that penalize the complexity of Gaussian random fields. *Journal of the American Statistical Association* 114, 445–452.
- Hahsler, M., Hornik, K., 2020. TSP: Traveling Salesperson Problem (TSP). URL: <https://CRAN.R-project.org/package=TSP>. R package version 1.1-10.
- 390 Husslage, B.G., Rennen, G., Van Dam, E.R., Den Hertog, D., 2011. Space-filling latin hypercube designs for computer experiments. *Optimization and Engineering* 12, 611–630.
- Illian, J.B., Sørbye, S.H., Rue, H., 2012. A toolbox for fitting complex spatial point process models using integrated nested laplace approximation (inla). *The Annals of Applied Statistics* , 1499–1530.
- Johnson, D., Laake, J., VerHoef, J., 2014. DSpat: Spatial Modelling for Distance Sampling Data. URL: <https://CRAN.R-project.org/package=DSpat>. R package version 0.1.6.
- 400 Kelly, F.P., Ripley, B.D., 1976. A note on Strauss's model for clustering. *Biometrika* 63, 357–360.
- Lark, R., 2016. Multi-objective optimization of spatial sampling. *Spatial Statistics* 18, 412–430.
- Lindgren, F., Rue, H., Lindström, J., 2011. An explicit link between Gaussian fields and Gaussian Markov random fields: the stochastic partial differential equation approach. *Journal of the Royal Statistical Society: Series B (Statistical Methodology)* 73, 423–498.
- 405 Liu, J., Vanhatalo, J., 2020. Bayesian model based spatiotemporal survey designs and partially observed log Gaussian Cox process. *Spatial statistics* 35, 100392.

- Ma, Q., Zhang, Y., 2016. Mechanics of fractal-inspired horseshoe microstructures for applications in stretchable electronics. *Journal of Applied Mechanics* 83.
- Matzke, B., Wilson, J., Newburn, L., Dowson, S., Hathaway, J., Sego, L.,
415 Bramer, L., Pulsipher, B., 2014. Visual Sample Plan Version 7.0 User's Guide. Pacific Northwest National Laboratory. Richland, Washington. URL: <http://vsp.pnnl.gov/docs/PNNL-23211.pdf>.
- McKay, M.D., Beckman, R.J., Conover, W.J., 1979. Comparison of three methods for selecting values of input variables in the analysis of output from a computer code. *Technometrics* 21, 239–245.
420
- Møller, J., Syversveen, A.R., Waagepetersen, R.P., 1998. Log Gaussian Cox processes. *Scandinavian journal of statistics* 25, 451–482.
- Ogorzałek, M.J., 2009. Fundamentals of fractal sets, space-filling curves and their applications in electronics and communications, in: Intelligent Computing Based on Chaos. Springer, pp. 53–72.
425
- Pollard, J., Palka, D., Buckland, S., 2002. Adaptive line transect sampling. *Biometrics* 58, 862–870.
- R Core Team, 2019. R: A Language and Environment for Statistical Computing. R Foundation for Statistical Computing. Vienna, Austria. URL: <https://www.R-project.org/>.
430
- Rue, H., Martino, S., Chopin, N., 2009. Approximate Bayesian inference for latent Gaussian models by using integrated nested Laplace approximations. *Journal of the royal statistical society: Series b (statistical methodology)* 71, 319–392.
- Sagan, H., 1994. Space-filling curves. Springer.
435
- Simpson, D., Illian, J.B., Lindgren, F., Sørbye, S.H., Rue, H., 2016. Going off grid: Computationally efficient inference for log-Gaussian Cox processes. *Biometrika* 103, 49–70.

- Simpson, D., Rue, H., Riebler, A., Martins, T.G., Sørbye, S.H., et al., 2017.
- 440 Penalising model component complexity: A principled, practical approach to
constructing priors. *Statistical science* 32, 1–28.
- Strauss, D.J., 1975. A model for clustering. *Biometrika* 62, 467–475.
- USACE, 2015. Technical Guidance for Military Munitions Response Actions. Technical Report EM 200-1-15. United States Army Corps of Engineers. URL: http://www.publications.usace.army.mil/Portals/76/Publications/EngineerManuals/EM_200-1-15.pdf.
- 445 Yuan, Y., Bachl, F.E., Lindgren, F., Borchers, D.L., Illian, J.B., Buckland, S.T.,
Rue, H., Gerrodette, T., et al., 2017. Point process models for spatio-temporal
distance sampling data from a large-scale survey of blue whales. *The Annals
of Applied Statistics* 11, 2270–2297.
- 450